

The dynamics of learning with feedback alignment

Maria Refinetti^{*1}, Stéphane d'Ascoli^{*1,2}, Ruben Ohana^{1,3} and Sebastian Goldt^{†4}

¹Laboratoire de Physique de l'Ecole Normale Supérieure, Université PSL, CNRS, Sorbonne Université, Université Paris-Diderot, Sorbonne Paris Cité, Paris, France

²Facebook AI Research, Paris, France

³LightOn, Paris, France

⁴International School of Advanced Studies (SISSA), Trieste, Italy

Abstract

Direct Feedback Alignment (DFA) is emerging as an efficient and biologically plausible alternative to the ubiquitous backpropagation algorithm for training deep neural networks. Despite relying on random feedback weights for the backward pass, DFA successfully trains state-of-the-art models such as Transformers. On the other hand, it notoriously fails to train convolutional networks. An understanding of the inner workings of DFA to explain these diverging results remains elusive. Here, we propose a theory for the success of DFA. We first show that learning in shallow networks proceeds in two steps: an *alignment* phase, where the model adapts its weights to align the approximate gradient with the true gradient of the loss function, is followed by a *memorisation* phase, where the model focuses on fitting the data. This two-step process has a *degeneracy breaking* effect: out of all the low-loss solutions in the landscape, a network trained with DFA naturally converges to the solution which maximises gradient alignment. We also identify a key quantity underlying alignment in deep linear networks: the conditioning of the *alignment matrices*. The latter enables a detailed understanding of the impact of data structure on alignment, and suggests a simple explanation for the well-known failure of DFA to train convolutional neural networks. Numerical experiments on MNIST and CIFAR10 clearly demonstrate degeneracy breaking in deep non-linear networks and show that the align-then-memorize process occurs sequentially from the bottom layers of the network to the top.

1 Introduction

Training a deep neural network on a supervised learning task requires solving the credit assignment problem: how should weights deep in the network be changed, given only the output of the network and the target label of the input? Today, almost all networks from computer vision to natural language processing solve this problem using variants of the back-propagation algorithm (BP) popularised several decades ago by Rumelhart *et al.* [1]. For concreteness, let us illustrate BP using a fully-connected deep network of depth L with weights W_l in the l th layer. Given an input $x \equiv h_0$, the output \hat{y} of the network is computed sequentially as $\hat{y} = f_y(a_L)$, with $a_l = W_l h_{l-1}$ and $h_l = g(a_l)$, where g is a pointwise non-linearity. For regression, the loss function J is the mean-square error and f_y is the identity. Given the error $e \equiv \partial J / \partial a_L = \hat{y} - y$ of the network on an input x , the update of the last layer of weights reads

$$\delta W_L = -\eta e h_{L-1}^\top \quad (1)$$

for a learning rate η . The updates of the layers below are given by $\delta W_l = -\eta \delta a_l h_{l-1}^\top$, with factors δa_l defined sequentially as

$$\delta a_l^{\text{BP}} = \partial J / \partial a_l = (W_{l+1}^\top \delta a_{l+1}) \odot g'(a_l), \quad (2)$$

^{*}Equal contribution

[†]sebastian.goldt@sissa.it

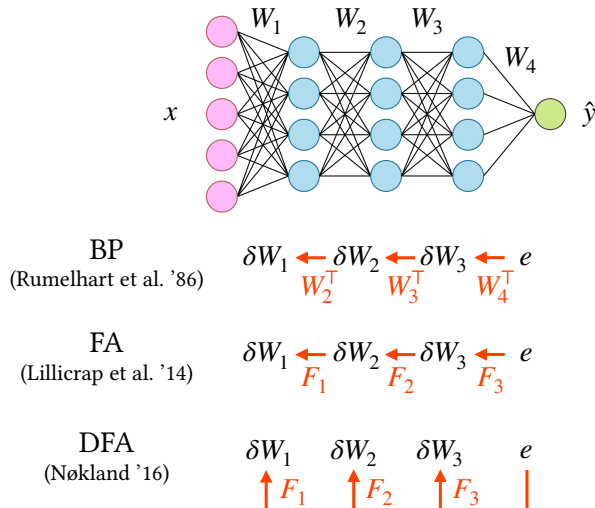


Figure 1: **Three approaches to the credit assignment problem in deep neural networks.** In *back-propagation* (BP), the weight updates δW_l are computed sequentially by transmitting the error e from layer to layer using the transpose of the network’s weights W_l^\top . In *feedback alignment* (FA) [4], W_l^\top are replaced by fixed random feedback matrices F_l . In *direct feedback alignment* (DFA) [5], the error is directly injected to each layer using random feedback matrices F_l , enabling parallelized training.

with \odot denoting the Hadamard product. BP thus solves the credit assignment problem for deeper layers of the network by using the transpose of the network’s weight matrices to transmit the error signal across the network from one layer to the next, see Fig. 1.

Despite its popularity and practical success, BP suffers from several limitations. First, it relies on symmetric weights for the forward and backward pass, which makes it an improbable candidate for a biologically plausible learning algorithm [2, 3]. Second, BP requires layers to be updated sequentially during the backward pass. Sequential updating prevents an efficient parallelisation of training, which becomes ever more important as state-of-the-art networks grow larger and deeper.

In light of these shortcomings, algorithms which only approximate the gradient of the loss are attracting increasing interest. Lillicrap *et al.* [4] demonstrated that neural networks can be trained successfully even if the transpose of the network weights W_l^\top are replaced by *random* feedback connections F_l in the backward pass, an algorithm they called “feedback alignment” (FA):

$$\delta a_l^{\text{FA}} = (F_l \delta a_{l+1}) \odot g'(a_l). \quad (3)$$

In this way, they dispense with the need of biologically unrealistic symmetric forward and backward weights [2, 3]. The “direct feedback alignment” (DFA) algorithm of Nøkland [5] takes this idea one step further by propagating the error directly from the output layer to each hidden layer of the network through random feedback connections F_l :

$$\delta a_l^{\text{DFA}} = (F_l e) \odot g'(a_l). \quad (4)$$

DFA thus allows updating different layers in parallel. We show the information flow of all three algorithms in Fig. 1.

While it was initially unclear whether DFA could scale to challenging datasets and complex architectures [6, 7], recently Launay *et al.* [8] obtained performances comparable to fine-tuned BP when using DFA to train a number of state-of-the-art architectures on problems ranging from neural view synthesis to natural language processing. Yet, feedback alignment still notoriously fails to train convolutional networks [7, 9–11]. These varied results underline the need for a theoretical understanding of how and when feedback alignment works.

Related Work A first theoretical characterisation of feedback alignment was provided by Lillicrap *et al.* [4], who showed that for two-layer linear networks, FA works because the transpose of the second layer of weights W_2 tends to align with the random feedback matrix F_1 during training. This *weight alignment* (WA) leads the weight updates of FA to align with those of BP, leading to *gradient alignment* (GA) and thus to successful learning. Frenkel *et al.* [12] extended this analysis to the deep linear case for a variant of DFA called “Direct Random Target Projection” (DRTP), under the restrictive assumption of training on a single data point. Nøkland [5] also introduced a layerwise alignment criterion to describe DFA in the deep nonlinear setup, under the assumption of constant update directions for each data point.

Contributions

1. We give an analytical description of DFA dynamics in shallow non-linear networks, building on seminal work analysing BP in the limit of infinitely many training samples [13–15].
2. We show that in this setup, DFA proceeds in two steps: an alignment phase, where the forward weights adapt to the feedback weights to improve the approximation of the gradient, is followed by a memorisation phase, where the network sacrifices some alignment to minimise the loss. Out of the same-loss-solutions in the landscape, DFA thus converges to the one that maximises gradient alignment, an effect we term “degeneracy breaking”.
3. We then focus on the alignment phase in the setup of deep linear networks, and uncover a key quantity underlying GA: the conditioning of the alignment matrices. Our framework allows us to analyse the impact of data structure on DFA, and suggests an explanation for the failure of DFA to train convolutional layers.
4. We complement our theoretical results with experiments that demonstrate the occurrence of (i) the Align-then-Memorise phases of learning, (ii) degeneracy breaking and (iii) layer-wise alignment in deep neural networks trained on standard vision datasets.

Reproducibility We host all the code to reproduce our experiments online at <https://github.com/sdascoli/dfa-dynamics>.

2 A two-phase learning process

We begin with an exact description of DFA dynamics in shallow non-linear networks. Here we consider a high-dimensional scalar regression task where the inputs $x \in \mathbb{R}^N$ are sampled i.i.d. from the standard normal distribution. We focus on the classic *teacher-student* setup, where the labels $y \in \mathbb{R}$ are given by the outputs of a “teacher” network with random weights [16–20]. In this section, we let the input dimension $N \rightarrow \infty$, while both teacher and student are two-layer networks with $K, M \sim O(1)$ hidden nodes. We consider sigmoidal, $g(x) = \text{erf}(x/\sqrt{2})$, and ReLU activation functions, $g(x) = \max(0, x)$. The key quantity of interest is the *generalisation error*, or test error, of the student,

$$\epsilon_g(\theta, \tilde{\theta}) \equiv \frac{1}{2} \mathbb{E} [\hat{y} - y]^2 \equiv \frac{1}{2} \mathbb{E} [e^2], \quad (5)$$

where the expectation \mathbb{E} is taken over the inputs for a given teacher and student networks with parameters $\tilde{\theta} = (M, \tilde{W}_1, \tilde{W}_2, g)$ and $\theta = (K, W_1, W_2, g)$. Learning a target function such as the teacher is a widely studied setup in the theory of neural networks [21–33].

In this shallow setup, FA and DFA are equivalent, and only involve one feedback matrix, which due to the scalar nature of the output is in fact a vector $F_1 \in \mathbb{R}^K$, which back-propagates the error signal e to the first layer weights W_1 . The updates of the second layer of weights W_2 are the same as for BP.

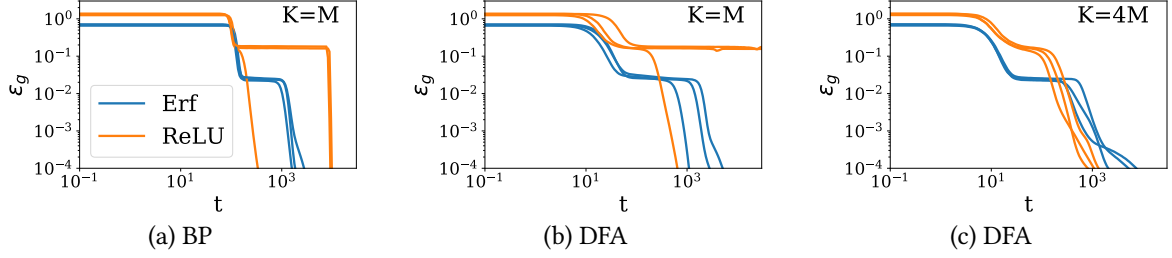


Figure 2: **Learning dynamics of back-propagation and feedback alignment for sigmoidal and ReLU neural networks learning a target function.** Each plot shows three runs from different initial conditions for every setting, where a shallow neural network with K hidden nodes tries to learn a teacher network with M hidden nodes. (a) All networks trained using BP in the matched case $K = M$ achieve perfect test error. (b) Sigmoidal networks achieve perfect test error with DFA, but the algorithm fails in some instances to train ReLU networks ($K = M$) (c) In the over-parametrised case ($K > M$), both sigmoidal and ReLU networks achieve perfect generalisation when trained with DFA. *Parameters:* $N = 500, L = 2, M = 2, \eta = 0.1, \sigma_0 = 10^{-2}$.

Performance of BP vs. DFA We show the evolution of the test error (5) of sigmoidal and ReLU students trained via vanilla BP in the “matched” case $K = M$ in Fig. 2 a, for three random choices of the initial weights with standard deviation $\sigma_0 = 10^{-2}$. In all cases, learning proceeds in three phases: an initial exponential decay; a phase where the error stays constant, the “plateau” [13, 19, 31]; and finally another exponential decay towards zero test error.

Sigmoidal students trained by DFA achieve perfect generalisation starting from different initial weights with a different feedback vector each time (blue in Fig. 2 b). This observation raises a first question: if the student has to align its second-layer weights with the random feedback vector in order to retrieve the true gradient [4], i.e. $W_2 \propto F_1$, how can it achieve perfect recovery of the teacher weights, i.e. $W_2 = \tilde{W}_2$?

For ReLU networks, over-parametrisation is key to the consistent success of DFA: while some students with $K = M$ fail to reach zero test error (orange in Fig. 2 b), almost every ReLU student that has more parameters than her teacher learns perfectly ($K = 4M$ in Fig. 2 c). The second question is thus: how does over-parameterisation help ReLU students achieve zero test error?

An analytical theory for DFA dynamics To answer these two questions, we study the dynamics of DFA in the limit of infinite training data where a previously unseen sample (x, y) is used to compute the DFA weight updates (4) at every step. This “online learning” or “one-shot/single-pass” limit of BP has been widely studied in recent and classical works of vanilla BP [13–15, 21, 34–40].

Our analysis concerns the regime where the input dimension $N \rightarrow \infty$, while M and K are finite. We start from the classic observation that the test error (5), a function of the student and teacher parameters involving a high-dimensional average over inputs, can be simply expressed in terms of a *finite* number of so-called “order parameters” $Q = (Q^{kl}), R = (R^{km}), T = (T^{mn})$,

$$\lim_{N \rightarrow \infty} \epsilon_g(\theta, \tilde{\theta}) = \epsilon_g(Q, R, T, W_2, \tilde{W}_2) \quad (6)$$

where

$$Q^{kl} = \frac{W_1^k W_1^l}{N}, \quad R^{km} = \frac{W_1^k \tilde{W}_1^m}{N}, \quad T^{mn} = \frac{\tilde{W}_1^m \tilde{W}_1^n}{N} \quad (7)$$

as well as second layer weights \tilde{W}_2^m and W_2^k [13–15, 19]. Intuitively, R^{km} quantifies the overlap or the similarity between the weights of the k th hidden unit of the student and the m th hidden unit of the teacher. The self-overlap of the k th and l th student nodes is given by Q^{kl} , and likewise T^{mn} gives the (static) self-overlap of teacher nodes. In seminal work, Saad & Solla [13] and Biehl & Schwarze [15] obtained a closed set of ordinary differential equations (ODEs) for the time evolution of the order

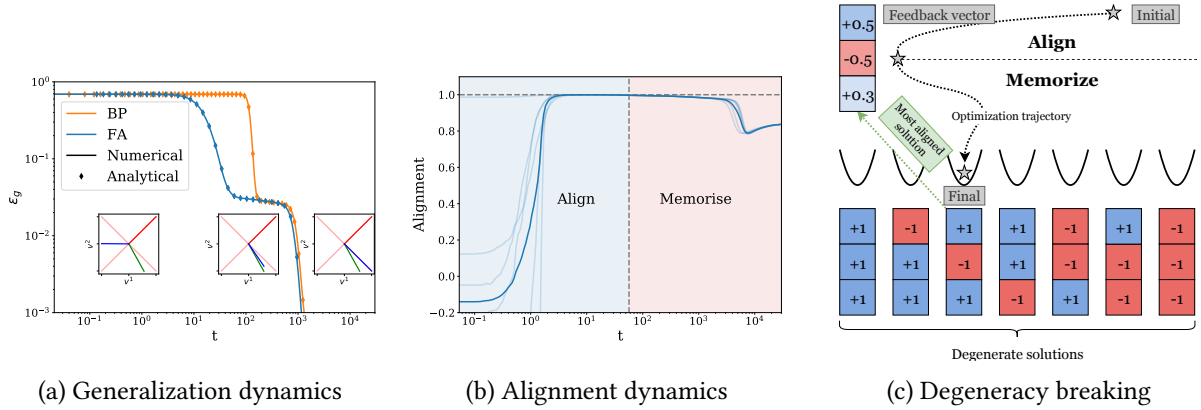


Figure 3: (a) **Theory gives exact prediction for the learning dynamics.** We plot learning curves for BP and DFA obtained from (i) a single simulation (solid lines), (ii) integration of the ODEs for BP dynamics [13, 15] (orange dots), (iii) integration of the ODEs for DFA derived here (blue dots). *Insets:* Teacher second-layer weights (red) as well as the degenerate solutions (light red) together with the feedback vector F (green) and the student second-layer weights v (blue) at three different times during training with DFA. *Parameters:* $N = 500$, $K = M = 2$, $\eta = 0.1$, $\sigma_0 = 10^{-2}$.

(b) **Align-then-Memorise process.** Alignment (cosine similarity) between the student’s second layer weights and the feedback vector. In the align phase, the alignment increases, and reaches its maximal value when the test loss reaches the plateau. Then it decreases in the memorization phase, as the student recovers the teacher weights.

(c) **The degeneracy breaking mechanism.** There are multiple degenerate global minima in the optimisation landscape: they are related through a discrete symmetry transformation of the weights that leaves the student’s output unchanged. DFA chooses the solution which maximises the alignment with the feedback vector.

parameters Q and R . Our first main contribution is to extend their approach to the DFA setup (see SM A for the details), obtaining a set of ODEs (A.6) that predicts the test error of a student trained using DFA (4) at all times. We demonstrate the accuracy of the predictions from the ODEs in Fig. 3 a, where we compare a single simulation of training a two-layer net with BP (orange) and DFA (blue) to the theoretical prediction for the test error, finding perfect agreement.

2.1 Sigmoidal networks learn through “degeneracy breaking”

The test loss of a sigmoidal student trained on a teacher with the same number of neurons as herself ($K = M$) contains several global minima, which all correspond to fixed points of the ODEs (A.6). One such global minimum corresponds to a student with exactly the same weights as her teacher, but the symmetry $\text{erf}(z) = -\text{erf}(-z)$ for any z means that a sigmoidal student with weights $\{\tilde{W}_1, \tilde{W}_2\}$ has the same test error as a sigmoidal student with weights $\{-\tilde{W}_1, -\tilde{W}_2\}$, so the problem of learning a teacher has various degenerate solutions, which we illustrate in Fig. 3 c. A student trained with vanilla BP will converge to any one of these solutions, depending on the initial conditions.

Alignment phase A student trained using DFA has to fulfil the same objective (zero test error), with the additional constraint that her second-layer weights W_2 need to align with the feedback vector F_1 to ensure that the first-layer weights are updated in the direction that minimises the test error. And indeed, a detailed analysis of the ODEs (cf. Sec. B) reveals that in the early phase of training, $\tilde{W}_2 \sim F$ and so W_2 grows in the direction of the feedback vector F_1 such that the overlap between W_2 and F_1 increases. This is the *alignment phase* of learning shown in Fig. 3 b. As W_2 and F_1 become perfectly aligned, DFA has perfectly recovered the weight updates for W_1 of BP, but the second layer has lost its expressivity (it is simply aligned to the random feedback vector).

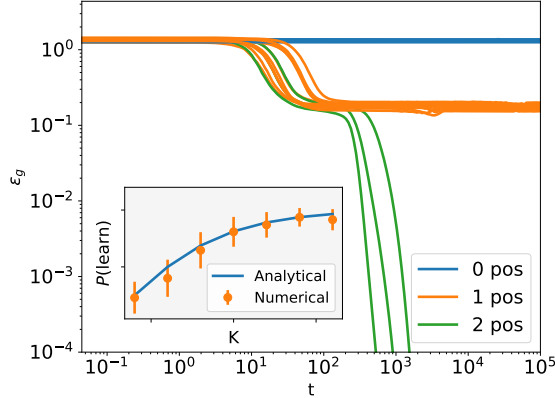


Figure 4: **Over-parameterisation improves performance of shallow ReLU networks.** We show the learning dynamics of a student with $K = 3$ hidden nodes trained on a teacher with $M = 2$ nodes and $\tilde{W}_2^m = 1$ if the feedback vector has 0, 1, or 2 positive entries. *Inset:* Probability of achieving zero test error (Eq. 8, line) compared to the fraction of simulations that converged to zero test error (out of 50, crosses). *Other parameters:* $N = 500, \eta = 0.1, \sigma_0 = 10^{-2}$.

Memorisation phase The expressivity of the student is restored in the *memorisation* phase of learning, where the second layer weights move away from F and towards the global minimum of the test error that maintains the highest overlap with the feedback vector. In other words, the student naturally converges to the solution for which the DFA gradient is the most aligned with the BP gradient. We found that students solve this constrained optimisation problem by consistently converging to the global minimum of the test loss that simultaneously maximises the overlap between W_2 and F_1 . For DFA, the global minima of the test loss are thus not equivalent, and we illustrate this “degeneracy breaking” in Fig. 3 c.

2.2 Degeneracy breaking requires over-parametrisation for ReLU networks

The ReLU activation function possesses the continuous symmetry $\max(0, x) = \gamma \max(0, x/\gamma)$ for any $\gamma > 0$. ReLU networks thus cannot compensate a change of sign of W_2^k with a change of sign of W_1^k . Hence, a ReLU student can only simultaneously align to the feedback vector F and recover the teacher’s second layer \tilde{W}_2 if at least M elements of F have the same sign as \tilde{W}_2 . This is illustrated in Fig. 4: a student trained on a teacher with $M = 2$ second-layer weights $\tilde{W}_2^m = 1$ only converges to zero test error if the feedback vector has 2 positive elements (green). If instead the feedback vector has only 0 (blue) or 1 (orange) positive entry, it will settle at a finite test error. Interestingly, the importance of the “correct” sign for the feedback matrices was also observed in deep neural networks by Liao *et al.* [41]. We describe this type of degeneracy breaking in more detail in Sec. B. The probability of perfect recovery for a student with $K \geq M$ nodes can be written as

$$P_{\text{learn}} = \frac{1}{2^K} \sum_{k=0}^M \binom{K}{k}, \quad (8)$$

which agrees well with simulations (inset of Fig. 4).

2.3 Degeneracy breaking in deep networks

To what extent does degeneracy breaking occur in deep nonlinear networks? We studied this question by training 4-layer multi-layer perceptrons (MLPs) with 100 nodes per layer for 1000 epochs with both BP and DFA, on the MNIST and CIFAR10 datasets, with Tanh and ReLU nonlinearities (cf. App. E.2 for

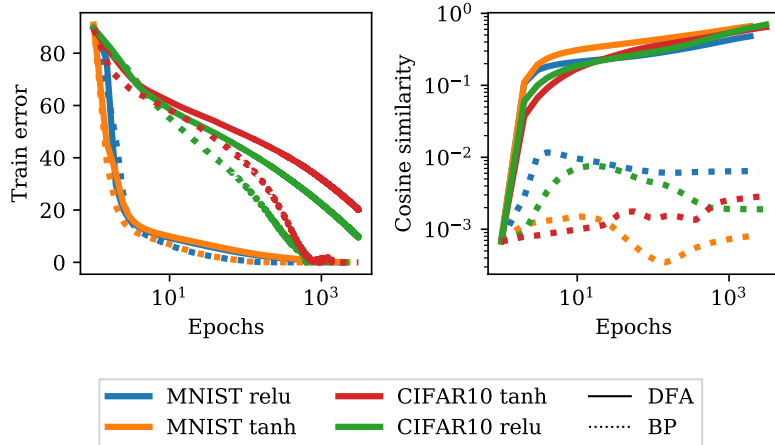


Figure 5: **Degeneracy breaking also occurs in deep neural networks.** We plot the training accuracy and the cosine similarity between the weights of four-layer fully-connected neural networks with sigmoidal and ReLU activations during training on MNIST and CIFAR10. Averages taken over 10 runs; for exp. details see Sec. 2.3.

further experimental details). The dynamics of the training loss, shown in the left of Fig. 5, are very similar for BP and DFA.

If degeneracy breaking holds, one expects DFA to drive the optimization path towards a special region of the loss landscape determined by the feedback matrices. We test this hypothesis by measuring whether networks trained from different initial weights but using the same feedback matrices converge towards the same region of the landscape. We compute the cosine similarity between the vectors obtained by stacking the weights of such networks at various times during training. The cosine similarity between two networks trained independently using BP reaches at most 10^{-2} (right of Fig. 5), signalling that they reach very distinct minima.

On the other hand, the cosine similarity of networks trained with DFA reached values between $0.5 - 1$ after training. This confirms our hypothesis that DFA breaks the degeneracy between the solutions in the landscape and biases towards a special region of the loss landscape, both for sigmoidal and ReLU activation functions. It also suggests that the reason heavily over-parametrised neural networks used in practice can be trained successfully with DFA is precisely because they have a large number of degenerate solutions. However, we leave a more detailed exploration of the interplay between DFA and the loss landscape for future work.

The more detailed experiments of Sec. 4 reveal that the Align-then-Memorise mechanism sketched in Fig. 3 c also appears in deep non-linear networks. Before discussing these results however, we first need to analyse the dynamics of alignment in deep networks.

3 How do gradients align in deep networks?

The focus of this section is on the alignment phase of learning. In the two-layer setup, alignment is simple: there is a single feedback vector F_1 , which has the same dimensions as the second layer W_2 , and to which W_2 must align in order for the first layer to recover the true gradient. In deep networks, each layer W_l has its own feedback matrix F_l , which has a different shape than W_l in DFA, so it is not obvious how the weights must align to ensure gradient alignment. We study how the alignment occurs by considering deep linear networks with L layers without bias, without making any assumption on the training data. While the expressivity of linear networks is naturally limited, their learning dynamics is non-linear and rich enough to give insights that carry over to the non-linear case both for BP [22, 42–45] and for DFA [4, 5, 12].

3.1 Weight alignment as a natural structure

We assume in the following analysis that the weights are set to zero at initialization. With BP, they would stay zero at all times, but thanks to DFA the layers become nonzero sequentially, from the bottom layer to the top layer. In the linear setup, the updates of the first two layers at time t can easily be written in terms of the corresponding input and error vectors using Eq. (4)¹:

$$\delta W_1^t = -\eta(F_1 e_t) x_t^T, \quad \delta W_2^t = -\eta(F_2 e_t)(W_1 x_t)^T \quad (9)$$

Summing these updates shows that the first layer performs Hebbian learning modulated by the feedback matrix F_1 :

$$W_1^t = -\eta \sum_{t'=0}^{t-1} F_1 e_{t'} x_{t'}^T = F_1 A_1^t, \quad (10)$$

$$A_1^t = -\eta \sum_{t'=0}^{t-1} e_{t'} x_{t'}^T \quad (11)$$

Plugging this result into δW_2^t , we can obtain the dynamics of W_2^t :

$$W_2^t = -\eta \sum_{t'=0}^{t-1} F_2 e_t (A_1^{t'} x_{t'})^T F_1^T = F_2 A_2^t F_1^T, \quad (12)$$

$$A_2^t = \eta^2 \sum_{t'=0}^{t-1} \sum_{t''=0}^{t'-1} (x_{t'} \cdot x_{t''}) e_{t'} e_{t''}^T. \quad (13)$$

Iterating the procedure above, we see that DFA naturally leads to *weak weight alignment* of the network weights to the feedback matrices in the following form:

$$\textbf{Weak WA: } W_{1 < l < L}^t = F_l A_l^t F_{l-1}^T, \quad W_L^t = A_L^t F_{L-1}^T, \quad (14)$$

where the *alignment matrices* $A_{l \geq 2}^t \in \mathbb{R}^{n_L \times n_L}$ are defined as:

$$A_{l \geq 2}^t = \eta^2 \sum_{t'=0}^{t-1} \sum_{t''=0}^{t'-1} (B_l^{t'} x_{t'}) \cdot (B_l^{t''} x_{t''}) e_{t'} e_{t''}^T. \quad (15)$$

Here, $B_l \in \mathbb{R}^{n_L \times n_L}$ is defined recursively as a function of the feedback matrices only. The full derivation as well as the expression for B_l 's are deferred to App. C. Note that one can specialize these results to DRTP [12], another variant of feedback alignment where $e_t = -y_t$. We can also easily adapt these results to FA by performing the replacement $F_l \rightarrow F_l F_{l+1} \dots F_{L-1}$.

3.2 Weight alignment leads to gradient alignment

Weak WA is naturally ensured when the weights are initialised from zero, and builds throughout training otherwise, but it does not directly imply GA. However, if the alignment matrices become proportional to the identity, we obtain *strong weight alignment*:

$$\textbf{Strong WA: } W_{1 < l < L}^t \propto F_l F_{l-1}^T, \quad W_L^t \propto F_{L-1}^T. \quad (16)$$

If we additionally assume that the feedback matrices $F_{l \geq 2}$ are left-orthogonal, i.e. $F_l^T F_l = \mathbb{I}_{n_L}$, strong WA directly implies GA. We can see this by comparing Eqs. 4 and 2, which imply that GA requires

¹We implicitly assume a minibatch size of 1 for notational simplicity, but conclusions are unchanged in the finite-batch setup.

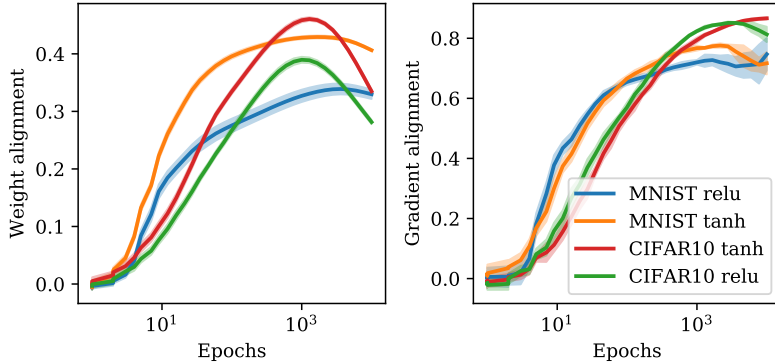


Figure 6: **Global alignment dynamics of deep nonlinear networks exhibits Align-then-Memorise.** Global weight and gradient alignments, as defined in (19), varying the activation function and the dataset. Shaded regions represent the (small) variability over 10 runs.

$F_l e \propto W_{l+1}^\top \delta a_{l+1}$. Thanks to the strong WA of (16), the weights cancel out by pairs of two due to the orthogonality condition

$$W_{l+1}^\top \delta a_{l+1} = \left[\prod_{l'=l+1}^L W_{l'}^\top \right] e \quad (17)$$

$$\propto F_l F_{l+1}^\top F_{l+1} \dots F_{L-1}^\top F_{L-1} e = F_l e. \quad (18)$$

This result suggests that taking the feedback matrices left-orthogonal is favorable for GA, but if we instead sample the feedback matrices elements i.i.d. from a Gaussian distribution, the GA will still hold in expectation since $\mathbb{E} [F_l^\top F_l] \propto \mathbb{I}_{n_L}$.

Quantifying gradient alignment Our analysis shows that the alignment matrices are the key quantities underlying GA: the closer they are to identity, i.e. the better their conditioning, the stronger the GA. However, this comes at the price of restricted expressivity, since it encourages layers to align to a product of (random) feedback matrices. In the extreme case of strong WA, layers $l \geq 2$ completely sacrifice their freedom to enable learning in the first layer! This is not harmful for the linear networks we considered, since the first layer alone is enough to maintain full expressivity². Nonlinear networks, on the other hand, rely on the Degeneracy Breaking mechanism to recover expressivity, as was shown in Sec. 2.

4 The case of deep nonlinear networks

In the two previous sections, we considered shallow nonlinear networks to demonstrate the Align-then-Memorise mechanism, then deep linear networks to study the weight alignment process at play during the alignment phase. In this section, we show that our theoretical predictions hold remarkably well in deep nonlinear networks trained on standard vision datasets.

4.1 Weight Alignment occurs like in the linear setup

To determine whether WA described in Sec. 3 holds in the deep nonlinear setup of Sec. 2.3, we introduce the global and layerwise alignment observables:

$$\text{WA} = \angle(\mathbf{F}, \mathbf{W}), \quad \text{GA} = \angle(\mathbf{G}^{\text{DFA}}, \mathbf{G}^{\text{BP}}) \quad (19)$$

$$\text{WA}_{l \geq 2} = \angle(\mathbf{F}_l, \mathbf{W}_l), \quad \text{GA}_{l \geq 2} = \angle(\mathbf{G}_l^{\text{DFA}}, \mathbf{G}_l^{\text{BP}}), \quad (20)$$

²such an alignment was indeed already observed in the linear setup for BP [46].

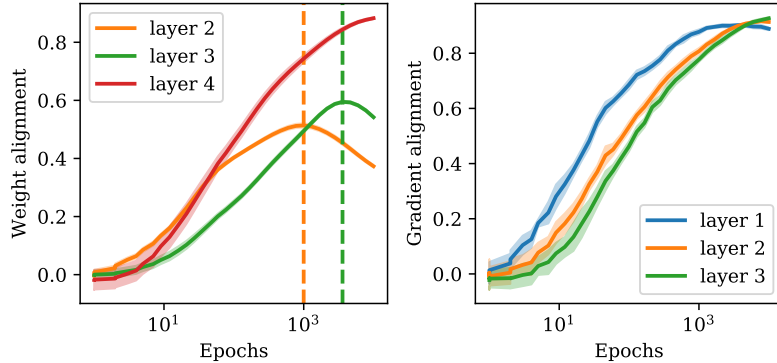


Figure 7: **Layerwise alignment dynamics reveal sequential Align-then-Memorise.** Layerwise weight and gradient alignments as defined in (20), for a ReLU network trained on CIFAR10 with 10% label corruption. Shaded regions represent the (small) variability over 10 runs.

where $\angle(\mathbf{A}, \mathbf{B}) = \text{Vec}(\mathbf{A}) \cdot \text{Vec}(\mathbf{B}) / \|\mathbf{A}\| \|\mathbf{B}\|$ and

$$\begin{aligned} \mathbf{F} &= \left(F_2 F_1^\top, \dots, F_{L-1} F_{L-2}^\top, F_{L-1}^\top \right), \\ \mathbf{W}(t) &= (W_2^t, \dots, W_{L-1}^t, W_L^t), \\ \mathbf{G}(t) &= (\delta a_1^t, \dots, \delta a_{L-1}^t). \end{aligned}$$

Note that the layer-wise alignment of W_l with $F_l F_{l-1}^\top$ was never measured before: it differs from the alignment of F_l with $W_{l+1} \dots W_L$ observed in [47], which is more akin to GA.

If \mathbf{W} and \mathbf{F} were uncorrelated, the WA defined in (19) would be vanishing as the width of the layer grows large. Remarkably, WA becomes of order one after a few epochs as shown in Fig. 6 (left), and strongly correlates with GA (right). This suggests that the layer-wise WA uncovered for linear networks with weights initialized to zero also drives GA in the general case.

4.2 Align-then-Memorise occurs from bottom layers to top

As can be seen in Fig. 6, WA clearly reaches a maximum then decreases, as expected from the Align-then-Memorise process. Notice that the decrease is stronger for CIFAR10 than it is for MNIST, since CIFAR-10 is much harder to fit than MNIST: more WA needs to be sacrificed. Increasing label corruption similarly makes the datasets harder to fit, and decreases the final WA, as detailed in SM E.2. However, another question arises: why does the GA keep increasing in this case, in spite of the decreasing WA?

To answer this question, we need to disentangle the dynamics of the layers of the network, as in Eq. (20). In Fig. 7, we focus on the ReLU network applied to CIFAR10, and shuffle 10% of the labels in the training set to make the Align-then-Memorise procedure more easily visible. Although the network contains 4 layers of weights, we only have 3 curves for WA and GA: WA is only defined for layers 2 to 4 according to Eq. (20), whereas GA of the last layer is not represented here since it is always equal to one.

As can be seen, the second layer is the first to start aligning: it reaches its maximal WA around 1000 epochs (orange dashed line), then decreases. The third layer starts aligning later and reaches its maximal WA around 2000 epochs (green dashed line), then decreases. As for the last layer, the WA is monotonically increasing. Hence, the Align-then-Memorise mechanism operates in a layerwise fashion, starting from the bottom layers to the top layers.

Note that the WA of the last layers is the most crucial, since it affects the GA of all the layers below, whereas the WA of the second layer only affects the GA of the first layer. It therefore makes sense to keep the WA of the last layers high, and let the bottom layers perform the memorization first. This is reminiscent of the linear setup, where all the layers align except for the first, which does all the learning. In fact, this strategy enables the GA of each individual layer to keep increasing until late times: the diminishing WA of the bottom layers is compensated by the increasing WA of the top layers.

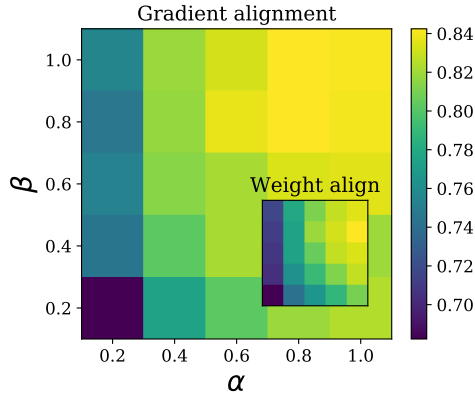


Figure 8: **Badly conditioned output statistics can hamper alignment.** WA and GA at the final point of training decrease when the output classes are correlated ($\beta < 1$) or of different variances ($\alpha < 1$).

5 What can hamper alignment?

We demonstrated that GA is enabled by the WA mechanism, both theoretically for linear networks and numerically for nonlinear networks. In this section, we leverage our analysis of WA to identify situations in which GA fails.

5.1 Alignment is data-dependent

In the linear case, GA occurs if the alignment matrices presented in Sec. 3 are well conditioned. Note that if the output size n_L is equal to one, e.g. for scalar regression or binary classification tasks, then the alignment matrices are simply scalars, and GA is guaranteed. When this is not the case, one can obtain the deviation from GA by studying the expression of the alignment matrices (15). They are formed by summing outer products of the error vectors $e_t e_t^\top$, where $e_t = \hat{y}_t - y_t$. Therefore, good conditioning requires the different components of the errors to be uncorrelated and of similar variances. This can be violated by (i) the targets y , or (ii) the predictions \hat{y} .

(i) Structure of data The first scenario can be demonstrated in a simple regression task on i.i.d. Gaussian inputs $x \sim \mathbb{R}^{10}$. The targets $y \in \mathbb{R}^2$ are randomly sampled from the following distribution:

$$y \sim \mathcal{N}(0, \Sigma), \quad \Sigma = \begin{bmatrix} 1 & \alpha(1 - \beta) \\ \alpha(1 - \beta) & \alpha^2 \beta \end{bmatrix}, \quad \alpha, \beta \leq 1. \quad (21)$$

In Fig. 8, we show the final WA and GA of a 3-layer ReLU network trained for 10^3 epochs on 10^3 examples sampled from this distribution (further details in SM E.3). As predicted, imbalanced ($\alpha < 1$) or correlated ($\beta < 1$) target statistics hamper WA and GA. Note that the inputs also come into play in Eq. (15): a more detailed theoretical analysis of the impact of input and target statistics on alignment is deferred to SM D.

(ii) Effect of noise For classification tasks, the targets y are one-hot encodings whose statistics are naturally well conditioned. However, alignment can be degraded if the statistics of the predictions \hat{y} become correlated.

One can enforce such a correlation in CIFAR10 by shuffling a fraction p of the labels. The WA and GA dynamics of a 3-layer ReLU network are shown in Fig. 9. At high p , the network can only perform random guessing during the first few epochs, and assigns equal probabilities to the 10 classes. The correlated structure of the predictions prevents alignment until the network starts to fit the random labels: the predictions of the different classes then decouple and WA takes off, leading to GA.

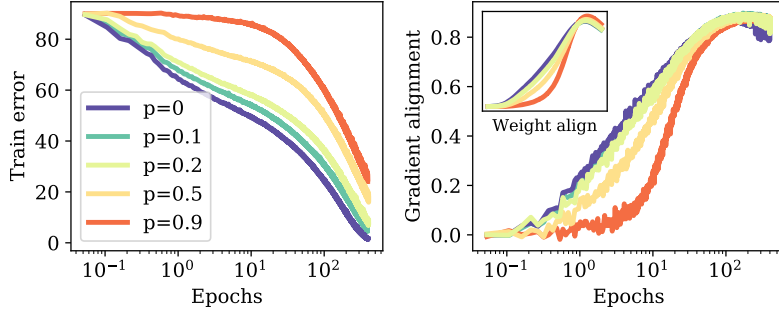


Figure 9: **Label corruption hampers alignment in the early stages of training.** We see that the higher the label corruption, the more time WA and GA take to start increasing, since the network initially predicts equal probabilities over the output classes.

5.2 Alignment is impossible for convolutional layers

A convolutional layer with filters H_l can be represented by a large fully-connected layer whose weights are represented by a block Toeplitz matrix $\phi(H_l)$ [48]. This matrix has repeated blocks due to weight sharing, and most of its weights are equal to zero due to locality. In order to verify WA and therefore GA, the following condition must hold: $\phi(H_l) \propto F_l F_l^\top$. Yet, due to the very constrained structure of $\phi(H_l)$, this is impossible for a general choice of F_l . Therefore, the WA mechanism suggests a simple explanation for why GA doesn't occur in vanilla CNNs, and confirms the previously stated hypothesis that CNNs don't have enough flexibility to align [10].

In the case of convolutional layers, this lack of alignment makes learning near to impossible, and has lead practitioners to design alternatives [9, 11]. However, the extent to which alignment correlates with good performance in the general setup (both in terms of fitting and generalisation) is a complex question which we leave for future work. Indeed, nothing prevents DFA from finding a good optimization path, different from the one followed by BP. Conversely, obtaining high gradient alignment at the end of training is not a sufficient condition for DFA to retrieve the results of BP, e.g. if the initial trajectory leads to a wrong direction.

Acknowledgements

We thank Florent Krzakala for introducing us to feedback alignment, and we thank him and Lenka Zdeborová for organising the Les Houches 2020 workshop on Statistical Physics and Machine Learning where this work was initiated. We thank Florent Krzakala, Giulio Biroli, Charlotte Frenkel, Julien Launay, Martin Lefebvre, Leonardo Petrini, Iacopo Poli, Levent Sagun and Mihiel Straat for helpful discussions. MR acknowledges funding from the French Agence Nationale de la Recherche under grant ANR-19-P3IA-0001 PRAIRIE. SD acknowledges funding from PRAIRIE for a visit to Trieste to collaborate on this project. RO acknowledges funding from the Region Ile-de-France.

A Derivation of the ODE

The derivation of the ODE's that describe the dynamics of the test error for shallow networks closely follows the one of Saad & Solla [13] and Biehl & Schwarze [15] for back-propagation. Here, we give the main steps to obtain the analytical curves of the main text and refer the reader to their paper for further details.

As we discuss in Sec. 2, student and teacher are both two-layer networks with K and M hidden nodes, respectively. For an input $x \in \mathbb{R}^N$, their outputs \hat{y} and y can be written as

$$\hat{y} = \phi_{\theta}(x) = \sum_{k=1}^K W_2^k g(\lambda^k), \quad y = \phi_{\tilde{\theta}}(x) = \sum_{m=1}^M \tilde{W}_2^m g(\nu^m), \quad (\text{A.1})$$

where we have introduced the pre-activations $\lambda^k \equiv W_1^k x / \sqrt{N}$ and $\nu^m \equiv \tilde{W}_1^m x / \sqrt{N}$. Evaluating the test error of a student with respect to the teacher under the squared loss leads us to compute the average

$$\epsilon_g(\theta, \tilde{\theta}) = \frac{1}{2} \mathbb{E}_x \left[\sum_{k=1}^K W_2^k g(\lambda^k) - \sum_{m=1}^M \tilde{W}_2^m g(\nu^m) \right]^2, \quad (\text{A.2})$$

where the expectation is taken over inputs x for a fixed student and teacher. Since x only enters Eq. (A.2) via the pre-activations $\lambda = (\lambda^k)$ and $\nu = (\nu^m)$, we can replace the high-dimensional average over x by a low-dimensional average over the $K + M$ variables (λ, ν) . The pre-activations are jointly Gaussian since the inputs are drawn element-wise i.i.d. from the Gaussian distribution. The mean of (λ, ν) is zero since $\mathbb{E} x_i = 0$, so the distribution of (λ, ν) is fully described by the second moments

$$Q^{kl} = \mathbb{E} \lambda^k \lambda^l = W_1^k \cdot W_1^l / N, \quad R^{km} = \mathbb{E} \lambda^k \nu^m = W_1^k \cdot \tilde{W}_1^m / N, \quad (\text{A.3})$$

$$T^{mn} = \mathbb{E} \nu^m \nu^n = \tilde{W}_1^m \cdot \tilde{W}_1^n / N. \quad (\text{A.4})$$

which are the ‘‘order parameters’’ that we introduced in the main text. We can thus rewrite the generalisation error (5) as a function of only the order parameters and the second-layer weights,

$$\lim_{N \rightarrow \infty} \epsilon_g(\theta, \tilde{\theta}) = \epsilon_g(Q, R, T, W_2, \tilde{W}_2) \quad (\text{A.5})$$

As we update the weights using SGD, the time-dependent order parameters Q , R , and W_2 evolve in time. By choosing different scalings for the learning rates in the SGD updates (4), namely

$$\eta_{W_1} = \eta, \quad \eta_{W_2} = \eta / N$$

for some constant η , we guarantee that the dynamics of the order parameters can be described by a set of ordinary differential equations, called their ‘‘equations of motion’’. We can obtain these equations in a heuristic manner by squaring the weight update (4) and taking inner products with \tilde{W}_1^m , to yield the equations of motion for Q and R respectively:

$$\frac{dR^{km}}{d\alpha} = -\eta F_1^k \mathbb{E} \left[g'(\lambda^k) \nu^m e \right] \quad (\text{A.6a})$$

$$\frac{dQ^{k\ell}}{d\alpha} = -\eta F_1^k \mathbb{E} \left[g'(\lambda^k) \lambda^\ell e \right] - \eta F_1^\ell \mathbb{E} \left[g'(\lambda^\ell) \lambda^k e \right] + \eta^2 F_1^k F_1^\ell \mathbb{E} \left[g'(\lambda^k) g'(\lambda^\ell) e^2 \right], \quad (\text{A.6b})$$

$$\frac{dW_2^k}{d\alpha} = -\eta \mathbb{E} \left[g(\lambda^k) e \right] \quad (\text{A.6c})$$

where, as in the main text, we introduced the error $e = \phi_{\theta}(x) - \phi_{\tilde{\theta}}(x)$. In the limit $N \rightarrow \infty$, the variable $\alpha = \mu / N$ becomes a continuous time-like variable. The remaining averages over the pre-activations, such as

$$\mathbb{E} g'(\lambda^k) \lambda^\ell g(\nu^m),$$

are simple three-dimensional integral over the Gaussian random variables λ^k , λ^ℓ and ν^m and can be evaluated analytically for the choice of $g(x) = \text{erf}(x/\sqrt{2})$ [15] and for linear networks with $g(x) = x$. Furthermore, these averages can be expressed only in term of the order parameters, and so the equations close. We note that the asymptotic exactness of Eqs. A.6 can be proven using the techniques used recently to prove the equations of motion for BP [29].

We provide an integrator for the full system of ODEs for any K and M in the Github repository.

B Detailed analysis of DFA dynamics

In this section, we present a detailed analysis of the ODE dynamics in the matched case $K = M$ for sigmoidal networks ($g(x) = \text{erf}(x/\sqrt{2})$).

The Early Stages and Gradient Alignment We now use Eqs. (A.6) to demonstrate that alignment occurs in the early stages of learning, determining from the start the solution DFA will converge to (see Fig. 3 which summarises the dynamical evolution of the student’s second layer weights).

Assuming zero initial weights for the student and orthogonal first layer weights for the teacher (i.e. T^{nm} is the identity matrix), for small times ($t \ll 1$), one can expand the order parameters in t :

$$R^{km}(t) = t\dot{R}^{km}(0) + \mathcal{O}(t^2), \quad Q^{kl}(t) = t\dot{Q}^{kl}(0) + \mathcal{O}(t^2), \quad W_2^k(t) = t\dot{W}_2^k(0) + \mathcal{O}(t^2). \quad (\text{B.1})$$

where, due to the initial conditions, $R(0) = Q(0) = W_2(0) = 0$. Using Eq. A.6, we can obtain the lowest order term of the above updates:

$$\dot{R}^{km}(0) = \frac{\sqrt{2}}{\pi}\eta\tilde{W}_2^m F_1^k, \quad \dot{Q}^{kl}(0) = \frac{2}{\pi}\eta^2 \left((\tilde{W}_2^k)^2 + (\tilde{W}_2^l)^2 \right) F_1^l F_1^k, \quad \dot{W}_2^k(0) = 0 \quad (\text{B.2})$$

Since both $\dot{R}(0)$ and $\dot{Q}(0)$ are non-zero, this initial condition is not a fixed point of DFA. To analyse initial alignment, we consider the first order term of \dot{W}_2 . Using Eq. (B.1) with the derivatives at $t = 0$ (B.2), we obtain to linear order in t :

$$\dot{W}_2^k(t) = \frac{2}{\pi^2}\eta^2 \|\tilde{W}_2\|^2 F_1^k t. \quad (\text{B.3})$$

Crucially, this update is in the direction of the feedback vector F_1 . DFA training thus constrains the student to initially grow in the direction of the feedback vector and align with it. This implies gradient alignment between BP and DFA and dictates into which of the many degenerate solutions in the energy landscape the student converges.

Plateau phase After the initial phase of learning with DFA where the test error decreases exponentially, similarly to BP, the student falls into a symmetric fixed point of the Eqs. (A.6) where the weights of a single student node are correlated to the weights of all the teacher nodes ([13, 15, 19]). The test error stays constant while the student is trapped in this fixed point. We can obtain an analytic expression for the order parameters under the assumption that the teacher first-layer weights are orthogonal ($T^{nm} = \delta_{nm}$). We set the teacher’s second-layer weights to unity for notational simplicity ($\tilde{W}_2^m = 1$) and restrict to linear order in the learning rate η , since this is the dominant contribution to the learning dynamics at early times and on the plateau [14]. In the case where all components of the feedback vector are positive, the order parameters are of the form $Q^{kl} = q$, $R^{km} = r$, $W_2^k = w_2$ with:

$$q = \frac{1}{2K-1}, \quad r = \sqrt{\frac{q}{2}}, \quad w_2 = \sqrt{\frac{1+2q}{q(4+3q)}}. \quad (\text{B.4})$$

If the components of the feedback vector are not all positive, we instead obtain $R^{km} = \text{sgn}(F^k)r$, $W_2^k = \text{sgn}(F^k)w_2$ and $Q^{kl} = \text{sgn}(F^k)\text{sgn}(F^l)q$. This shows that on the plateau the student is already in the configuration that maximises its alignment with F_1 . Note that in all cases, the value of the test error reached at the plateau is the same for DFA and BP.

Memorisation phase and Asymptotic Fixed Point At the end of the plateau phase, the student converges to its final solution, which is often referred to as the *specialised* phase [13, 15, 19]. The configuration of the order parameters is such that the student reproduces her teacher up to sign changes that guarantee the alignment between W_2 and F_1 is maximal, i.e. $\text{sgn}(W_2^k) = \text{sgn}(F_1^k)$. The final value of the test error of a student trained with DFA is the same as that of a student trained with BP on the same teacher.

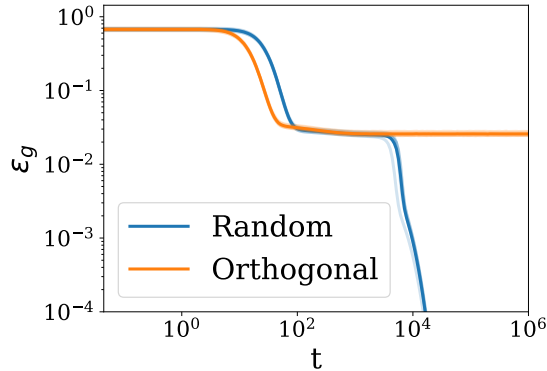


Figure 10: Test error of a sigmoidal student started with zero initial weights. The feedback vector F_1 is chosen random (blue) and orthogonal to the teacher’s second layer weights \tilde{W}_2 (orange). Parameters: $\eta = 0.1, K = M = 2$.

Choice of the feedback vector In the main text, we saw how a wrong choice of feedback vector F_1 can prevent a ReLU student from learning a task. Here, we show that also for sigmoidal student, a *wrong* choice of feedback vector F_1 is possible. As Fig. 10 shows, in the case where the F_1 is taken orthogonal to the teacher second layer weights, a student whose weights are initialised to zero remains stuck on the plateau and is unable to learn. In contrast, when the F_1 is chosen with random i.i.d. components drawn from the standard normal distribution, perfect recovery is achieved.

C Derivation of weight alignment

Since the network is linear, the update equations are (consider the first three layers only):

$$\delta W_1 = -\eta(F_1 e)x^T, \quad (\text{C.1})$$

$$\delta W_2 = -\eta(F_2 e)(W_1 x)^T, \quad (\text{C.2})$$

$$\delta W_3 = -\eta(F_3 e)(W_2 W_1 x)^T \quad (\text{C.3})$$

First, it is straightforward to see that

$$W_1^t = -\eta \sum_{t'=0}^{t-1} F_1 e_{t'} x_{t'}^T = F_1 A_1^t \quad (\text{C.4})$$

$$A_1^t = -\eta \sum_{t'=0}^{t-1} e_{t'} x_{t'}^T \quad (\text{C.5})$$

This allows to calculate the dynamics of W_2^t :

$$\delta W_2^t = -\eta F_2 e_t (A_1^t x_t)^\top F_1^\top \quad (\text{C.6})$$

$$W_2^t = -\eta \sum_{t'=0}^{t-1} F_2 e_{t'} (A_1^{t'} x_{t'})^\top F_1^\top = F_2 A_2^t F_1^\top \quad (\text{C.7})$$

$$A_2^t = -\eta \sum_{t'=0}^{t-1} e_{t'} (A_1^{t'} x_{t'})^\top = \eta^2 \sum_{t'=0}^{t-1} \sum_{t''=0}^{t'-1} (x_{t'} \cdot x_{t''}) e_{t'} e_{t''}^\top. \quad (\text{C.8})$$

which in turns allows to calculate the dynamics of W_3^t :

$$\delta W_3^t = -\eta F_3 e_t (F_2 A_2^t F_1^\top F_1 A_1^t x_t)^\top \quad (\text{C.9})$$

$$W_3^t = -\eta \sum_{t'=0}^{t-1} F_3 e_{t'} (F_2 A_2^{t'} F_1^\top F_1 A_1^{t'} x_{t'})^\top = F_3 A_3^t F_2^\top \quad (\text{C.10})$$

$$A_3^t = -\eta \sum_{t'=0}^{t-1} F_3 e_{t'} (A_2^{t'} F_1^\top F_1 A_1^{t'} x_{t'})^\top \quad (\text{C.11})$$

$$= \eta^2 \sum_{t'=0}^{t-1} \sum_{t''=0}^{t'-1} (A_1^{t'} x_{t'}) \cdot (A_1^{t''} x_{t''}) e_{t'} e_{t''}^\top. \quad (\text{C.12})$$

By induction it is easy to show the general expression:

$$A_1^t = -\eta \sum_{t'=0}^{t-1} e_{t'} x_{t'}^\top \quad (\text{C.13})$$

$$A_2^t = \eta^2 \sum_{t'=0}^{t-1} \sum_{t''=0}^{t'-1} (x_{t'} \cdot x_{t''}) e_{t'} e_{t''}^\top \quad (\text{C.14})$$

$$A_{l \geq 3}^t = \eta^2 \sum_{t'=0}^{t-1} \sum_{t''=0}^{t'-1} (A_{l-2}^{t'} \cdots A_1^{t'} x_{t'}) \cdot (A_{l-2}^{t''} \cdots A_1^{t''} x_{t''}) e_{t'} e_{t''}^\top \quad (\text{C.15})$$

Defining $A_0 \equiv \mathbb{I}_{n_0}$, one can rewrite this as in Eq. 15

$$A_{l \geq 2}^t = \eta^2 \sum_{t'=0}^{t-1} \sum_{t''=0}^{t'-1} (B_l^{t'} x_{t'}) \cdot (B_l^{t''} x_{t''}) e_{t'} e_{t''}^\top, \quad (\text{C.16})$$

$$B_l = A_{l-2} \cdots A_0. \quad (\text{C.17})$$

D Impact of data structure

To study the impact of data structure on the alignment, the simplest setup to consider is that of Direct Random Target Projection [12]. Indeed, in this case the error vector $e_t = -y_t$ does not depend on the prediction of the network: the dynamics become explicitly solvable in the linear case.

For concreteness, we consider the setup of [4] where the targets are given by a linear teacher, $y = Tx$, and the inputs are i.i.d Gaussian. We denote the input and target correlation matrices as follows:

$$\mathbb{E} [xx^\top] \equiv \Sigma_x \in \mathbb{R}^{n_0 \times n_0}, \quad (\text{D.1})$$

$$\mathbb{E} [TT^\top] \equiv \Sigma_y \in \mathbb{R}^{n_L \times n_L} \quad (\text{D.2})$$

If the batch size is large enough, one can write $x_t x_t^\top = \mathbb{E}[x x^\top] = \Sigma_x$. Hence the dynamics of Eq. 9 become:

$$\delta W_1^t = -\eta(F_1 e_t) x_t^\top = \eta F_1 T x_t x_t^\top = \eta F_1 T \Sigma_x \quad (\text{D.3})$$

$$\delta W_2^t = -\eta(F_2 e_t)(W_1 x_t)^\top = \eta F_2 T \Sigma_x W_1^\top \quad (\text{D.4})$$

$$= \eta^2 F_2 \left(T \Sigma_x^2 T^\top \right) F_1^\top \quad (\text{D.5})$$

$$\delta W_3^t = -\eta(F_3 e_t)(W_2 W_1 x_t)^\top = \eta F_3 T \Sigma_x W_1^\top W_2^\top \quad (\text{D.6})$$

$$= \eta^3 F_3 \left(T \Sigma_x^2 T^\top \right) \left(T \Sigma_x^2 T^\top \right) F_2^\top \quad (\text{D.7})$$

From which we easily deduce $A_1^t = \eta T \Sigma_x t$, and the expression of the alignment matrices at all times:

$$A_{l \geq 2}^t = \eta^l \left(T \Sigma_x^2 T^\top \right)^{l-1} t \quad (\text{D.8})$$

As we saw, GA depends on how well-conditioned the alignment matrices are, i.e. how different it is from the identity. To examine deviation from identity, we write $\Sigma_x = \mathbb{I}_{n_0} + \tilde{\Sigma}_x$ and $\Sigma_y = \mathbb{I}_{n_L} + \tilde{\Sigma}_y$, where the tilde matrices are small perturbations. Then to first order,

$$A_{l \geq 2}^t - I_{n_L} \propto (l-1) \left(\tilde{\Sigma}_y + 2T \tilde{\Sigma}_x T^\top \right) \quad (\text{D.9})$$

Here we see that GA depends on how well-conditioned the input and target correlation matrices Σ_x and Σ_y are. In other words, if the different components of the inputs or the targets are correlated or of different variances, we expect GA to be hampered, observed in Sec. 5. Note that due to the $l-1$ exponent, we expect poor conditioning to have an even more drastic effect in deeper layers.

Notice that in this DRTP setup, the norm of the weights grows linearly with time, which makes DRTP inapplicable to regression tasks, and over-confident in classification tasks. It is clear in this case the the first layer learns the teacher, and the subsequent layers try to passively transmit the signal.

E Details about the experiments

E.1 Direct Feedback Alignment implementation

We use the Pytorch implementation of DFA implemented in [8], accessible at <https://github.com/lightonai/dfa-scales-to-modern-deep-learning>. Note that we do not use the shared feedback matrix trick introduced in this work. We sample the elements of the feedback matrix F_l from a centered uniform distribution of scale $1/\sqrt{n_l + 1}$.

E.2 Experiments on realistic datasets

We trained 4-layer MLPs with 100 nodes per layer for 1000 epochs using vanilla SGD, with a batch size of 32 and a learning rate of 10^{-4} . The datasets considered are MNIST and CIFAR10, and the activation functions are Tanh and ReLU.

We initialise the networks using the standard Pytorch initialization scheme. We do not use any momentum, weight decay, dropout, batchnorm or any other bells and whistles. We downscale all images to 14×14 pixels to speed up the experiments. Results are averaged over 10 runs.

For completeness, we show in Fig. 11 the results in the main text for 4 different levels of label corruption. The transition from Alignment phase to Memorisation phase can clearly be seen in all cases from the drop in weight alignment. Three important remarks can be made:

- **Alignment phase:** Increasing label corruption slows down the early increase of weight alignment, as noted in Sec. 5.1.

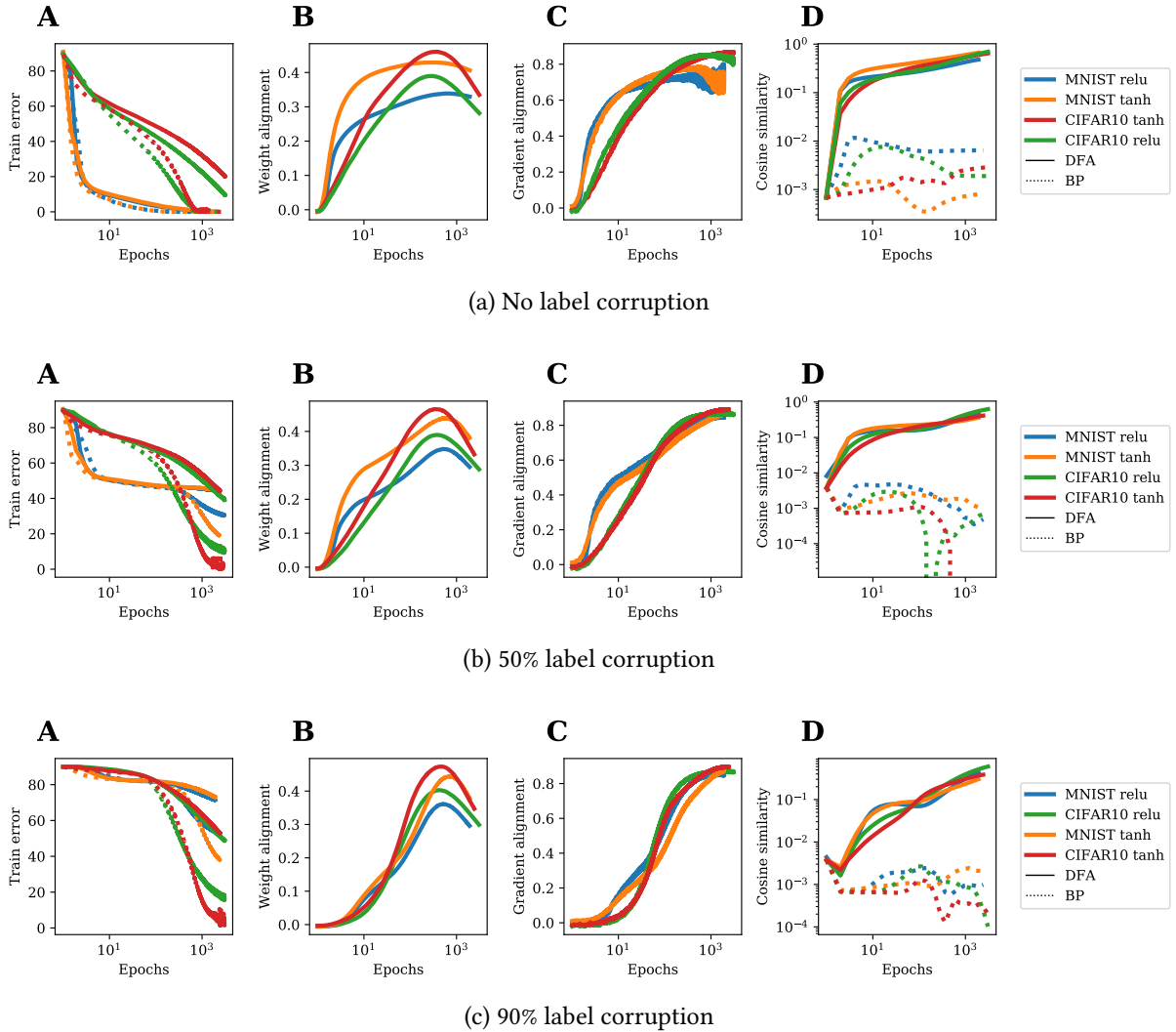


Figure 11: Effect of label corruption on training observables. **A**: Training error. **B** and **C**: Weight and gradient alignment, as defined in the main text. **D**: Cosine similarity of the weight during training.

- **Memorization phase**: Increasing label corruption makes the datasets harder to fit. As a consequence, the network needs to give up more weight alignment in the memorization phase, as can be seen from the sharper drop in the weight alignment curves.
- **Transition point**: the transition time between the Alignment and Memorization phases coincides with the time at which the training error starts to decrease sharply (particularly at high label corruption), and is hardly affected by the level of label corruption.

E.3 Experiment on the structure of targets

We trained a 3-layer linear MLP of width 100 for 1000 epochs on the synthetic dataset described in the main text, containing 10^4 examples. We used the same hyperparameters as for the experiment on nonlinear networks. We choose 5 values for α and β : 0.2, 0.4, 0.6, 0.8 and 1.

In Fig. 12, we show the dynamics of weight alignment for both ReLU and Tanh activations. We again see the Align-then-Memorise process distinctly. Notice that decreasing α and β hampers both the maximal weight alignment (at the end of the alignment phase) and the final weight alignment (at the end of the memorisation phase).

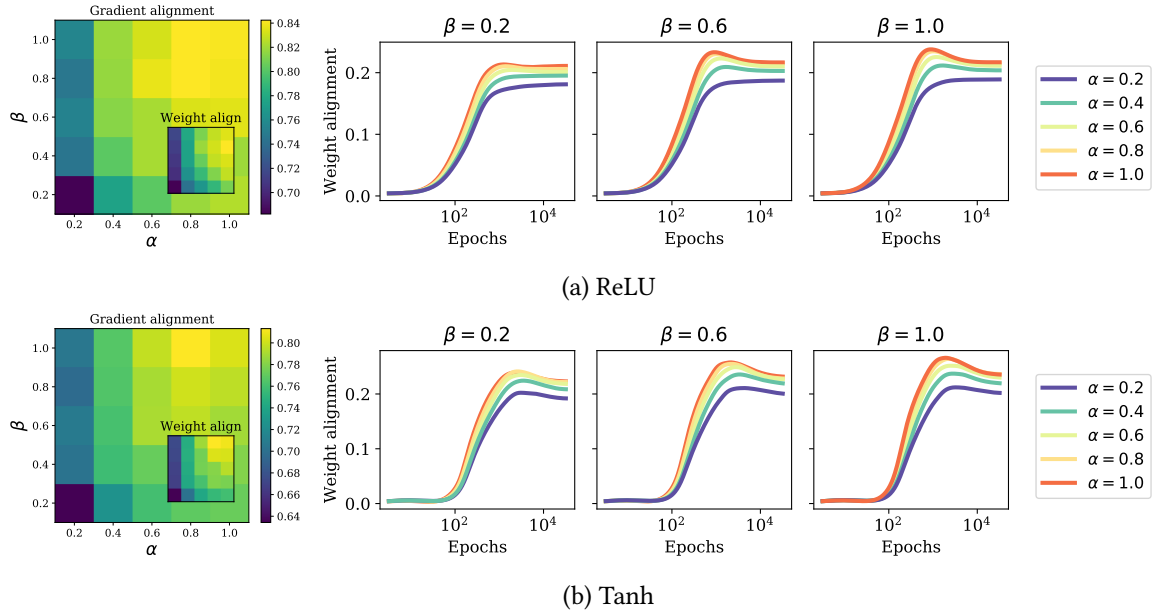


Figure 12: WA is hampered when the output dimensions are correlated ($\beta < 1$) or of different variances ($\alpha < 1$).

References

1. Rumelhart, D. E., Hinton, G. E. & Williams, R. J. Learning representations by back-propagating errors. *Nature* **323**, 533–536 (1986).
2. Grossberg, S. Competitive learning: From interactive activation to adaptive resonance. *Cognitive science* **11**, 23–63 (1987).
3. Crick, F. The recent excitement about neural networks. *Nature* **337**, 129–132 (1989).
4. Lillicrap, T., Cownden, D., Tweed, D. & Akerman, C. Random synaptic feedback weights support error backpropagation for deep learning. *Nature Communications* **7**, 1–10 (2016).
5. Nøkland, A. *Direct Feedback Alignment Provides Learning in Deep Neural Networks* in *Advances in Neural Information Processing Systems* **29** (2016).
6. Gilmer, J., Raffel, C., Schoenholz, S. S., Raghu, M. & Sohl-Dickstein, J. *Explaining the learning dynamics of direct feedback alignment* in *ICLR workshop track* (2017).
7. Bartunov, S. *et al.* *Assessing the scalability of biologically-motivated deep learning algorithms and architectures* in *Advances in Neural Information Processing Systems* (2018), 9368–9378.
8. Launay, J., Poli, I., Boniface, F. & Krzakala, F. *Direct Feedback Alignment Scales to Modern Deep Learning Tasks and Architectures* in *Advances in neural information processing systems* (2020).
9. Moskovitz, T. H., Litwin-Kumar, A. & Abbott, L. Feedback alignment in deep convolutional networks. *arXiv preprint arXiv:1812.06488* (2018).
10. Launay, J., Poli, I. & Krzakala, F. Principled Training of Neural Networks with Direct Feedback Alignment. *arXiv:1906.04554* (2019).
11. Han, D. & Yoo, H.-j. *Direct Feedback Alignment Based Convolutional Neural Network Training for Low-Power Online Learning Processor* in *Proceedings of the IEEE International Conference on Computer Vision Workshops* (2019).
12. Frenkel, C., Lefebvre, M. & Bol, D. *Learning without feedback: Direct random target projection as a feedback-alignment algorithm with layerwise feedforward training* 2019. arXiv: [1909.01311](https://arxiv.org/abs/1909.01311).

13. Saad, D. & Solla, S. Exact Solution for On-Line Learning in Multilayer Neural Networks. *Phys. Rev. Lett.* **74**, 4337–4340 (1995).
14. Saad, D. & Solla, S. On-line learning in soft committee machines. *Phys. Rev. E* **52**, 4225–4243 (1995).
15. Biehl, M. & Schwarze, H. Learning by on-line gradient descent. *J. Phys. A: Math. Gen.* **28**, 643–656 (1995).
16. Gardner, E. & Derrida, B. Three unfinished works on the optimal storage capacity of networks. *Journal of Physics A: Mathematical and General* **22**, 1983–1994 (1989).
17. Seung, H. S., Sompolinsky, H. & Tishby, N. Statistical mechanics of learning from examples. *Physical Review A* **45**, 6056–6091 (1992).
18. Watkin, T., Rau, A. & Biehl, M. The statistical mechanics of learning a rule. *Reviews of Modern Physics* **65**, 499–556 (1993).
19. Engel, A. & Van den Broeck, C. *Statistical mechanics of learning* (Cambridge University Press, 2001).
20. Zdeborová, L. & Krzakala, F. Statistical physics of inference: thresholds and algorithms. *Adv. Phys.* **65**, 453–552 (2016).
21. Zhong, K., Song, Z., Jain, P., Bartlett, P. & Dhillon, I. *Recovery guarantees for one-hidden-layer neural networks* in *Proceedings of the 34th International Conference on Machine Learning-Volume 70* (2017), 4140–4149.
22. Advani, M. S., Saxe, A. M. & Sompolinsky, H. High-dimensional dynamics of generalization error in neural networks. *Neural Networks* **132**, 428–446 (2020).
23. Tian, Y. *An Analytical Formula of Population Gradient for Two-Layered ReLU Network and Its Applications in Convergence and Critical Point Analysis* in *Proceedings of the 34th International Conference on Machine Learning (ICML)* (2017), 3404–3413.
24. Du, S., Lee, J., Tian, Y., Singh, A. & Póczos, B. *Gradient Descent Learns One-hidden-layer CNN: Don't be Afraid of Spurious Local Minima* in *Proceedings of the 35th International Conference on Machine Learning* **80** (2018), 1339–1348.
25. Soltanolkotabi, M., Javanmard, A. & Lee, J. Theoretical insights into the optimization landscape of over-parameterized shallow neural networks. *IEEE Transactions on Information Theory* **65**, 742–769 (2018).
26. Aubin, B. *et al.* *The committee machine: Computational to statistical gaps in learning a two-layers neural network* in *Advances in Neural Information Processing Systems 31* (2018), 3227–3238.
27. Saxe, A. *et al.* *On the information bottleneck theory of deep learning* in *ICLR* (2018).
28. Baity-Jesi, M. *et al.* *Comparing Dynamics: Deep Neural Networks versus Glassy Systems* in *Proceedings of the 35th International Conference on Machine Learning* (2018).
29. Goldt, S., Advani, M., Saxe, A., Krzakala, F. & Zdeborová, L. *Dynamics of stochastic gradient descent for two-layer neural networks in the teacher-student setup* in *Advances in Neural Information Processing Systems 32* (2019).
30. Ghorbani, B., Mei, S., Misiakiewicz, T. & Montanari, A. *Limitations of Lazy Training of Two-layers Neural Network* in *Advances in Neural Information Processing Systems 32* (2019), 9111–9121.
31. Yoshida, Y. & Okada, M. *Data-Dependence of Plateau Phenomenon in Learning with Neural Network — Statistical Mechanical Analysis* in *Advances in Neural Information Processing Systems 32* (2019), 1720–1728.
32. Bahri, Y. *et al.* *Statistical Mechanics of Deep Learning*. *Annual Review of Condensed Matter Physics* **11**, 501–528 (2020).
33. Gabrié, M. Mean-field inference methods for neural networks. *Journal of Physics A: Mathematical and Theoretical* **53**, 223002 (2020).

34. Kinzel, W. & Ruján, P. Improving a Network Generalization Ability by Selecting Examples. *EPL (Europhysics Letters)* **13**, 473–477 (1990).
35. Saad, D. *On-line learning in neural networks* (Cambridge University Press, 2009).
36. Brutzkus, A. & Globerson, A. Globally Optimal Gradient Descent for a ConvNet with Gaussian Inputs in *Proceedings of the 34th International Conference on Machine Learning - Volume 70* (2017), 605–614.
37. Mei, S., Montanari, A. & Nguyen, P. A mean field view of the landscape of two-layer neural networks. *Proceedings of the National Academy of Sciences* **115**, E7665–E7671 (2018).
38. Rotskoff, G. & Vanden-Eijnden, E. Parameters as interacting particles: long time convergence and asymptotic error scaling of neural networks in *Advances in Neural Information Processing Systems 31* (2018), 7146–7155.
39. Chizat, L. & Bach, F. On the Global Convergence of Gradient Descent for Over-parameterized Models using Optimal Transport in *Advances in Neural Information Processing Systems 31* (2018), 3040–3050.
40. Sirignano, J. & Spiliopoulos, K. Mean field analysis of neural networks: A central limit theorem. *Stochastic Processes and their Applications* (2019).
41. Liao, Q., Leibo, J. Z. & Poggio, T. How important is weight symmetry in backpropagation? in *Proceedings of the Thirtieth AAAI Conference on Artificial Intelligence* (2016), 1837–1844.
42. Baldi, P. & Hornik, K. Neural networks and principal component analysis: Learning from examples without local minima. *Neural networks* **2**, 53–58 (1989).
43. Le Cun, Y., Kanter, I. & Solla, S. A. Eigenvalues of covariance matrices: Application to neural-network learning. *Physical Review Letters* **66**, 2396 (1991).
44. Krogh, A. & Hertz, J. A. Generalization in a linear perceptron in the presence of noise. *Journal of Physics A: Mathematical and General* **25**, 1135 (1992).
45. Saxe, A., McClelland, J. & Ganguli, S. Exact solutions to the nonlinear dynamics of learning in deep linear neural networks in *International Conference on Learning Representations (ICLR)* (2014).
46. Ji, Z. & Telgarsky, M. Gradient descent aligns the layers of deep linear networks in *International Conference on Learning Representations (ICLR)* (2019).
47. Crafton, B., Parihar, A., Gebhardt, E. & Raychowdhury, A. Direct feedback alignment with sparse connections for local learning. *Frontiers in neuroscience* **13**, 525 (2019).
48. d’Ascoli, S., Sagun, L., Biroli, G. & Bruna, J. Finding the Needle in the Haystack with Convolutions: on the benefits of architectural bias in *Advances in Neural Information Processing Systems* (2019), 9334–9345.